SUPPLEMENTARY INFORMATION

MATERIALS AND METHODS

i/TIF34-b/PRT1 Affinity Analysis Using Gel Mobility Shift Assays.
The [^{35}S]-labeled C-terminal b/PRT1 peptides were prepared using the TnT coupled rabbit reticulocyte *in vitro* translation and transcription system (Promega). Proteins were synthesized by incubating 1 μg of plasmid in 40 μl of TnT Quick Master mixture with 2 μl of L-[^{35}S] methionine (Amersham Biosciences) for 2 hours at 25°C. The *in vitro* translated products were then purified using HIS-Select™ spin columns (Sigma) according to the manufacturer's instructions. Unlabeled C-terminal b/PRT1 peptides and i/TIF34 were expressed in *E. coli* and purified as above. Dissociation constant of b/PRT1(630-724) was determined by titrating purified [^{35}S]-b/PRT1 (0.1 μM final concentration) with increasing amount of purified i/ TIF34 (0, 0.1, 0.25, 0.5, 1.0, 5.0, 10, 25.0 μM final concentration) in a final volume of 20 μl reaction mix containing 20 mM Hepes pH 7.5, 50 mM NaCl and 5% glycerol. For competition assay, 0.2 μM#[^{35}S]-b/PRT1 (630-724) was first mixed with 1 μM i/TIF34, then unlabeled b/PRT1 peptides were added to increasing concentrations at the following ratios of unlabelled to labelled protein: 0.1, 0.5, 1, 10, 25, 50, 100 for b(630-724); 1, 2, 10, 25, 50, 100 for W674F; 1, 10, 25, 50, 100, 200 for W674A; 1, 10, 25, 50, 200 for Y677A/R68A; and 1, 5, 50, 100, 200 for b(654-700). Complexes were formed at 30°C and analyzed on 4-16% native polyacrylamide BisTris gels (Invitrogen). Gel electrophoresis was performed for 2 h at 100 V at 4 °C using NativePAGE running buffer (Invitrogen). Gels were then dried on Whatman paper and exposed overnight on a PhosphorImager screen. Bound and free radioactive b/PRT1 bands were quantified using ImageQuantTL image analysis tool. Data analysis was performed using DynaFit software (58,59). Direct and competition titration data were fit using equilibrium binding or displacement models for single site binding.

Calorimetry (ITC) Analysis of i/TIF34-b/PRT1 Interactions.
All calorimetric titrations were performed on a VP-ITC microcalorimeter (Microcal). Protein samples were dialyzed against the same storage/NMR buffer (see Materials and Methods in the main text). The sample cell was filled with 200 μl of 26 μM solution of i/TIF34 and the injection syringe with 288 μM or 200 μM of b/PRT1(654-700) or b/PRT1(630-724), respectively. Each titration typically consisted of a preliminary 0.5 μl injection followed by 20 subsequent 2-μl injections every 120 seconds. All of the experiments were performed at 25 °C. Data for the preliminary injection, which are affected by diffusion of the solution from and into the injection syringe during the initial equilibration period, were discarded. Binding isotherms were generated by plotting heats of reaction normalized by the moles of injectant versus the ratio of total injectant to total protein per injection. The data were fitted to single site binding model using Origin 7.0 (Microcal).

Yeast Genetic and Biochemical Methods.

GST pull-down assays with GST fusions and *in vitro*-synthesized [^{35}S]-labeled polypeptides were conducted as follows. Individual GST-fusion proteins were expressed in *E. coli*, immobilized on glutathione-Sepharose beads and incubated with 10 μl of [^{35}S]-labeled potential binding partners at 4°C for 2 h. The beads were washed 3 times with 1 ml of phosphate-buffered saline and bound proteins separated by SDS-PAGE. Gels were first stained with Gelcode Blue Stain Reagent (Pierce) and then subjected to autoradiography. Ni^{2+}-chelation chromatography of eIF3 complexes containing His_8-tagged b/PRT1 or g/TIF35 from yeast whole-cell extracts (WCEs) and Western blot analysis were conducted as described in detail previously (60). In short, WCEs were incubated with 15 μL of 50% Ni^{2+}-NTA-silica resin (GE Healthcare) suspended in 200 μL of buffer A for 2 h at 4°C, followed by washing and elution. 2% HCHO cross-linking followed by WCE preparation and fractionation of extracts for analysis of pre-initiation complexes were carried out as described previously (38). β-galactosidase assays were conducted as described previously (61).

Preparation of Antibodies Against RPS0A.

The GST-RPS0A fusion protein encoded by pGEX-RPS0A was expressed in *E. coli* and purified from the WCE by incubation with Glutathione-Sepharose 4B beads (Pharmacia). The isolated protein was resolved by SDS-PAGE (4-20% gels), excised from the gel, and washed with 1x PBS. Rabbits were injected with the purified protein and serum containing polyclonal antibodies against RPS0A was obtained commercially by Apronex (Prague, the Czech Republic).

Construction of Yeast Strains and Plasmids.

List of all strains named below can be found in Tables S3.

To create AY134 strain, YAH06 was transformed with pRS-b/PRT1-HisXS and the original covering plasmid carrying *PRT1 URA3* was evicted on 5-FOA.

YAH11 was generated by a genetic cross of H420 and AY134 as a haploid ascospore resistant to 3-AT, unable to grow on 5-FOA, unable to evict a resident *LEU2* covering plasmid, and autotrophic for tryptophan.

To create YAH12 strain, YAH11 was transformed with pCR52-1 (62) and grown on SD media containing Leucine to get rid of the original pRS-b/PRT1-HisXS plasmid.

List of all plasmids and PCR primers named below can be found in Tables S4 and S5, respectively.

pRS-b/PRT1-W674A-His was generated by fusion PCR. The following pairs of primers were used for separate PCR amplifications using pRS-b/PRT1-His as template: (1) AH-PRT1-BamHI and AH-PRT1-W674A-R, respectively, (2) AH-PRT1-W674A and AH-PRT1-NotI-R, respectively. The PCR products thus obtained were used in a 1:1 ratio as templates for a third PCR amplification using primers AH-PRT1-BamHI and AH-PRT1-NotI-R. The resulting PCR product was digested with BamHI and NotI and ligated with BamHI-NotI-cleaved pRS-b/PRT1-His.

pRS-b/PRT1-W674F-His – was generated by fusion PCR. The following pairs of primers were used for separate PCR amplifications using pRS-b/PRT1-His as template: (1) AH-PRT1-BamHI and AH-PRT1-W674F-R, respectively, (2) AH-PRT1-W674F and AH-PRT1-NotI-R, respectively. The PCR products thus obtained were used in a 1:1 ratio as templates for a third PCR amplification using primers AH-PRT1-BamHI and AH-PRT1-NotI-R. The resulting PCR product was digested with BamHI and NotI and ligated with BamHI-NotI-cleaved pRS-b/PRT1-His.

pRS-b/PRT1-Y677A-His was made by inserting the BamHI-MscI digested PCR product obtained with primers AH-PRT1-BamHI and AH-PRT1-Y677A-R using pRS-b/PRT1-HisXS as a template into BamHI-MscI digested pRS-b/PRT1-HisXS.

pRS-b/PRT1-R678A-His was made by inserting the BamHI-MscI digested PCR product obtained with primers AH-PRT1-BamHI and AH-PRT1-R678A-R using pRS-b/PRT1-HisXS as a template into BamHI-MscI digested pRS-b/PRT1-HisXS.

pRS-b/PRT1-Y677A-R678A-His was made by inserting the BamHI-MscI digested PCR product obtained with primers AH-PRT1-BamHI and AH-PRT1-YR-AA-R using pRS-b/PRT1-HisXS as a template into BamHI-MscI digested pRS-b/PRT1-HisXS.

pRS-b/PRT1-Y677A-R678D-His was made by inserting the BamHI-MscI digested PCR product obtained with primers AH-PRT1-BamHI and AH-PRT1-YR-AD-R using pRS-b/PRT1-HisXS as a template into BamHI-MscI digested pRS-b/PRT1-HisXS.

YCp-i/TIF34-D207K-HA was generated by fusion PCR. The following pairs of primers were used for separate PCR amplifications using YCp-i/TIF34-HA as template: (1) y3iKpnI and D207Kr, respectively, (2) D207K and BmgBIr, respectively. The PCR products thus obtained were used in a 1:1 ratio as templates for a third PCR amplification using primers y3iKpnI and BmgBIr. The resulting PCR product was digested with KpnI and BmgBI and ligated with KpnI-BmgBI-cleaved YCp-i/TIF34-HA.

YCp-i/TIF34-D224K-HA was generated by fusion PCR. The following pairs of primers were used for separate PCR amplifications using YCp-i/TIF34-HA as template: (1) y3iKpnI and D224Kr, respectively, (2) D224K and BmgBIr, respectively. The PCR products thus obtained were used in a 1:1 ratio as templates for a third PCR amplification using primers y3iKpnI and BmgBIr. The resulting PCR product was digested with KpnI and BmgBI and ligated with KpnI-BmgBI-cleaved YCp-i/TIF34-HA.

YCp-i/TIF34-D207K-D224K-HA was generated by fusion PCR. The following pairs of primers were used for separate PCR amplifications using YCp-i/TIF34-D207K-HA as template: (1) y3iKpnI and D224Kr, respectively, (2) D224K and BmgBIr, respectively. The PCR products thus obtained were used in a 1:1 ratio as templates for a third PCR amplification using primers y3iKpnI and BmgBIr. The resulting PCR product was digested with KpnI and BmgBI and ligated with KpnI-BmgBI-cleaved YCp-i/TIF34-D207K-HA.

YCp-i/TIF34-L222D-HA was generated by fusion PCR. The following pairs of primers were used for separate PCR amplifications using YCp-i/TIF34-HA as template: (1) y3iKpnI and LC3iLr, respectively, (2) LC3iL222D and BmgBIr, respectively. The PCR products thus obtained were used in a 1:1 ratio as templates for a third PCR amplification using primers y3iKpnI and BmgBIr. The resulting PCR product was digested with KpnI and BmgBI and ligated with KpnI-BmgBI-cleaved YCp-i/TIF34-HA.

YCp-i/TIF34-L222K-HA was generated by fusion PCR. The following pairs of primers were used for separate PCR amplifications using YCp-i/TIF34-HA as template: (1) y3iKpnI and LC3iLr, respectively, (2) LC3iL222K and BmgBIr, respectively. The PCR products thus obtained were used in a 1:1 ratio as templates for a third PCR amplification using primers y3iKpnI and BmgBIr. The resulting PCR product was digested with KpnI and BmgBI and ligated with KpnI-BmgBI-cleaved YCp-i/TIF34-HA.

YCp-i/TIF34-HA-W was constructed by inserting the 2223bp SacI-DrdI fragment from YCp-i/TIF34-HA into YCplac22 digested with SacI-DrdI.

YCp-i/TIF34-D207K-D224K-HA-W was constructed by inserting the 2223bp SacI-DrdI fragment from YCp-i/TIF34-D207K-D224K-HA into YCplac22 digested with SacI-DrdI.

YCp-i/TIF34-D207K-HA-W was constructed by inserting the 2223bp SacI-DrdI fragment from YCp-i/TIF34-D207K-HA into YCplac22 digested with SacI-DrdI.

YCp-i/TIF34-D224K-HA-W was constructed by inserting the 2223bp SacI-DrdI fragment from YCp-i/TIF34-D224K-HA into YCplac22 digested with SacI-DrdI.

YEp-g/TIF35-His was constructed by inserting the 2112bp EcoRI-PstI fragment from YCp-g/TIF35-His-screen into YEplac195 digested with EcoRI-PstI.

YEp-SUI1-G107R was constructed by inserting the 287bp BamHI-SacII fragment from pCFB134 into YEp-SUI1 digested with BamHI-SacII.

pT7-b/PRT1-W674A was constructed by inserting the 1222bp NsiI-MscI fragment from pRS-b/PRT1-W674A-His into pT7-b/PRT1 digested with NsiI-MscI.

pT7-b/PRT1-Y677A was constructed by inserting the 1222bp NsiI-MscI fragment from pRS-b/PRT1-Y677A-His into pT7-b/PRT1 digested with NsiI-MscI.

pT7-b/PRT1-R678A was constructed by inserting the 1222bp NsiI-MscI fragment from pRS-b/PRT1-R678A-His into pT7-b/PRT1 digested with NsiI-MscI.

pT7-i/TIF34-D207K-D224K was constructed by inserting the 587bp KpnI-EcoRI fragment from YCp-i/TIF34-D207K-D224K-HA into pT7-i/TIF34 digested with KpnI-EcoRI.

pGEX-RPS0A was constructed in two steps. First, the intron was removed by a fusion PCR using pGBK-RPS0A (37) as a template and the following pair of primers for two separate PCR reactions producing exon 1 (O1-BamHI x BSRPS0Aexon1-r) and exon2 (BSRPS0Aexon2 x O2-KpnI-XhoI-r), respectively. Both PCR products thus obtained were used in a 1:1 ratio as templates for a third PCR amplification using primers O1-BamHI and O2-KpnI-XhoI-r. The resulting PCR

product was digested with BamHI and XhoI and ligated with BamHI-XhoI-cleaved pGEX-4T-1 (63).

REFERENCES

58. Kuzmic, P., Michael, L.J. and Ludwig, B. (2009), *Methods in Enzymology*. Academic Press, Vol. Volume 467, pp. 247-280.
59. Kuzmic, P. (1996) Program DYNAFIT for the Analysis of Enzyme Kinetic Data: Application to HIV Proteinase. *Analytical Biochemistry*, **237**, 260-273.
60. Nielsen, K.H. and Valášek, L. (2007) In vivo deletion analysis of the architecture of a multi-protein complex of translation initiation factors. *Methods Enzymol.*, **431**, 15-32.
38. Valášek, L., Szamecz, B., Hinnebusch, A.G. and Nielsen, K.H. (2007) In Vivo Stabilization of Preinitiation Complexes by Formaldehyde Cross-Linking. *Methods Enzymol.*, **429**, 163-183.
61. Grant, C.M., Miller, P.F. and Hinnebusch, A.G. (1994) Requirements for intercistronic distance and level of eIF-2 activity in reinitiation on GCN4 mRNA varies with the downstream cistron. *Mol Cell Biol*, **14**, 2616-2628.
62. Cigan, A.M., Foiani, M., Hannig, E.M. and Hinnebusch, A.G. (1991) Complex formation by positive and negative translational regulators of *GCN4*. *Mol Cell Biol*, **11**, 3217-3228.
37. Valášek, L., Mathew, A., Shin, B.S., Nielsen, K.H., Szamecz, B. and Hinnebusch, A.G. (2003) The Yeast eIF3 Subunits TIF32/a and NIP1/c and eIF5 Make Critical Connections with the 40S Ribosome in vivo. *Genes Dev*, **17**, 786-799.
63. Smith, D.B. and Johnson, K.S. (1988) Single-step purification of polypeptides expressed in Escherichia coli as fusions with glutathione S-transferase. *Gene*, **67**, 31-40.
10. Asano, K., Phan, L., Anderson, J. and Hinnebusch, A.G. (1998) Complex formation by all five homologues of mammalian translation initiation factor 3 subunits from yeast *Saccharomyces cerevisiae*. *J Biol Chem*, **273**, 18573-18585.
29. Davis, I.W., Leaver-Fay, A., Chen, V.B., Block, J.N., Kapral, G.J., Wang, X., Murray, L.W., Arendall, W.B., III, Snoeyink, J., Richardson, J.S. *et al.* (2007) MolProbity: all-atom contacts and structure validation for proteins and nucleic acids. *Nucleic Acids Research*, **35**, W375-383.
35. Krissinel, E. and Henrick, K. (2007) Inference of Macromolecular Assemblies from Crystalline State. *J Mol Biol.*, **372**, 774-797.
12. ElAntak, L., Wagner, S., Herrmannová, A., Karásková, M., Rutkai, E., Lukavsky, P.J. and Valášek, L. (2010) The indispensable N-terminal half of eIF3j co-operates with its structurally conserved binding partner eIF3b-RRM and eIF1A in stringent AUG selection. *J Mol Biol.*, **396**, 1097-1116.
64. Gietz, R.D. and Sugino, A. (1988) New yeast-Escherichia coli shuttle vectors constructed with in vitro mutagenized yeast genes lacking six-base pair restriction sites. *Gene*, **74**, 527-534.
5. Cuchalová, L., Kouba, T., Herrmannová, A., Danyi, I., Chiu, W.-l. and Valášek, L. (2010) The RNA Recognition Motif of Eukaryotic Translation Initiation Factor 3g (eIF3g) Is Required for Resumption of Scanning of Posttermination Ribosomes for Reinitiation on GCN4 and Together with eIF3i Stimulates Linear Scanning. *Mol Cell Biol*, **30**, 4671-4686.

39. Valášek, L., Nielsen, K.H., Zhang, F., Fekete, C.A. and Hinnebusch, A.G. (2004) Interactions of Eukaryotic Translation Initiation Factor 3 (eIF3) Subunit NIP1/c with eIF1 and eIF5 Promote Preinitiation Complex Assembly and Regulate Start Codon Selection. *Mol. Cell. Biol.*, **24**, 9437-9455.
47. Cheung, Y.N., Maag, D., Mitchell, S.F., Fekete, C.A., Algire, M.A., Takacs, J.E., Shirokikh, N., Pestova, T., Lorsch, J.R. and Hinnebusch, A.G. (2007) Dissociation of eIF1 from the 40S ribosomal subunit is a key step in start codon selection in vivo. *Genes Dev*, **21**, 1217-1230.
13. Valášek, L., Phan, L., Schoenfeld, L.W., Valášková, V. and Hinnebusch, A.G. (2001) Related eIF3 subunits TIF32 and HCR1 interact with an RNA recoginition motif in PRT1 required for eIF3 integrity and ribosome binding. *EMBO J*, **20**, 891-904.

FIGURE LEGENDS

Figure S1. Identification of the minimal i/TIF34-binding site of b/PRT1. (**A**) Overlay of $^{1}H,^{15}N$-TROSY (transverse relaxation optimized spectroscopy) spectra of ^{13}C, ^{15}N-labelled b/PRT1(630-724) in the free form (purple) or bound to unlabelled i/TIF34 (pink). Assigned amide crosspeaks from bound b/PRT1(630-724) which display sharp resonance lines and random coil chemical shifts are labeled. The NεH side chain crosspeaks of W644 and W674, which resonate downfield of the backbone amide NH crosspeaks are shown in an inset. Only the W674-NεH resonances display large chemical changes upon i/TIF34 binding, while W644-NεH remains unchanged suggesting that the middle part if b/PRT1(630-724) comprises the i/TIF34 binding site. (**B**) Overlay of $^{1}H,^{15}N$-TROSY spectra of ^{15}N-labelled b/PRT1(630-724; purple) or ^{15}N-labelled b/PRT1(654-700; pink) both bound to unlabelled i/TIF34. The shorter b/PRT1 peptide lacks most of the sharp, random coil amide NH resonances from the longer b/PRT1 peptide, while very similar, broad amide NH resonances close to the noise level arising from i/TIF34-interacting parts of b/PRT1 are observed in both peptides. The Trp-NεH side chain crosspeaks are shown in an inset. The shorter b/PRT1 peptide (pink) lacks the sharp, random coil W644-NεH resonances of the longer peptide (purple), but displays the same broad, downfield-shifted crosspeak for W674-NεH as found for the longer peptide suggesting a very similar binding mode of both peptides. (**C**) Isothermal calorimetric titration of i/TIF34 with b/PRT1(630-724) and b/PRT1(654-700) reveal comparable binding affinities. The panels show experimental data and the fitted binding isotherms. The data was analyzed using Origin 7.0 (MicroCal) software. Data points were obtained by integration of heat signals plotted against the molar ratio of i/TIF34 to b/PRT1 variants in the reaction cell. The solid line represents a calculated curve using the best-fit parameters obtained by a nonlinear least squares fit. The b/PRT1 construct used for each experiment is indicated in the panel.

Figure S2. Sequence alignment of i/TIF34 and b/PRT1 from different species and stereo view of the i/TIF34 - b/PRT1 binding interface. (**A**) Sequence alignment of eIF3i/TIF34 and eIF3b/PRT1 from *S. cerevisiae*, human, *Drosophila*, frog, *Neurospora*, Mouse and *Arabidopsis*. Phylogenetic analysis reveals a high level of

eIF3i/TIF34 and eIF3b/PRT1 conservation between species. In eIF3b/PRT1, only the C-terminus is shown; blue triangles indicate boundaries of our eIF3b/PRT1 construct, residues important for the interaction and discussed in the text are numbered according to *S. cerevisiae*. Secondary structure elements are shown above the aligned sequences. (**B**) Interface of i/TIF34 and b/PRT1(654-700) interactions. i/TIF34 is in green, b/PRT1(654-700) in blue. Cross-eye stereo image was generated using PyMOL (http://www.pymol.org).

Figure S3. Structure of the i/TIF34-b/PRT1(654-700) complex. (**A**) Left, experimentally phased, solvent-flattened electron density map with the refined model superimposed. Right, part of the experimental electron density map in the region of b/PRT1(654-700). Protein backbones are shown as ribbons. (**B**) Overall view of the i/TIF34-b/PRT1(654-700) complex (two complexes in asymmetric unit) with the corresponding 2mFo-DFc electron density map shown contoured at 1 sigma. i/TIF34 is in green, b/PRT1(654-700) in blue. Ray-traced images were generated using PyMOL (http://www.pymol.org).

Figure S4. Two i/TIF34-b/PRT1 complexes are present in the asymmetric unit. i/TIF34 chains are shown in green, b/PRT1 in blue. Blades in the β-propeller structure of i/TIF34 are numbered from 1 to 7 (N to C-terminus). The two complexes in the asymmetric unit interact through the surface-exposed loop (residues 112-121 in blade 4) of one i/TIF34 molecule with β-sheet in blade 1 and loop in blade 2 of another i/TIF34 molecule, as depicted by the red arrow. Complex I denotes chains E and B, as named in the pdb file, and complex II – chains F and D.

Figure S5. Positional comparison of the i/TIF34 residues directly interacting with b/PRT1 with those identified in previous mutational studies by Asano and co-workers (10), which cluster on opposite sides of beta-propeller. Positions of eight lethal mutations are shown as red dots. The residues include Y18, C28, H51, D61, G257 (to D or S), G294 and D314. Ts^- changes at positions G311 and P247 are shown as blue dots. In the latter work, amino acids conferring Ts^- or Slg^- mutations were identified in blades 6 (*P247L* and *Q258R*) and 7 (*G311S*). Direct comparison shown here clearly reveals that none of these residues form contacts to b/PRT1(654-700). Mutations *P247L* and *G311S* were proposed to affect mainly binding of g/TIF35, since overexpression of g/TIF35 could fully suppress the observed phenotypes (10). Notably, P247 is in close proximity to the extended C-terminal part of b/PRT1 (starting with residue 689) suggesting that both b/PRT1 and g/TIF35 might share the same binding surface on i/TIF34. In agreement with this proposal, the Ts^- mutation *Q258R*, which was only weakly suppressed by the high copy *TIF35* plasmid and conferred no defects in binding to b/PRT1 or g/TIF35 (10), resides at the base of the flexible loop (residues 260-272) on the opposite site of the b/PRT1 binding site.

Figure S6. i/TIF34 residues 260-272 fold into a flexible loop. (**A**) The flexible loop within blade 6 (residues 260-272) displays well-defined electron density only in one

molecule of the asymmetric unit (complex II, chain D in the pdb file - shown with the corresponding 2mFo-DFc electron density map contoured at 1.0 sigma). The loop in another molecule (complex I, chain B) is not visible and therefore the residues have been omitted from the pdb file. The red arrow indicates the site of the lacking flexible loop in the complex I. (**B**) Side view showing the flexible loop (indicated by black bracket), which bears neutral-to-negative charge.

Figure S7. Gel shift analysis of i/TIF34 binding to b/PRT1 mutants. (**A**) b/PRT1(630-739) binds i/TIF34 with a K_D of 0.26 μM±0.15, as determined by directly titrating 0.1 μM [^{35}S]-b/PRT1 with increasing amounts of i/TIF34 (0.1-25 μM) and calculated using DynaFit software (58,59). (**B**) Competition assays were used to test binding of b/PRT1 mutants. 0.2 μM [^{35}S]-b/PRT1(630-724) was mixed with 1 μM i/TIF34, and increasing amounts of unlabeled b/PRT1 peptides were added to the reaction mixture (see Supplementary Materials and Methods). Complexes were incubated at 30°C temperature in a final volume of 20 μl reaction mix containing 20 mM Hepes pH 7.5, 50 mM NaCl and 5% glycerol for 20 min and analyzed on 4-16% native polyacrylamide BisTris gels (Invitrogen). The b/PRT1(654-700) peptide and W674F mutant bind i/TIF34 with similar affinity as the b/PRT1(630-724). The increments of increase (the ratio of concentrations of unlabeled to labeled proteins) were as follows: panel b(630-724): 0.1, 0.5, 1, 10, 25, 50, 100; panel W674F: 1, 2, 10, 25, 50, 100; panel W674A: 1, 10, 25, 50, 100, 200; panel Y677A/R678A: 1, 10, 25, 50, 200; panel b(654-700): 1, 5, 50, 100, 200.

Figure S8. (**A**) The *tif34-DD/KK* mutation disrupts i/TIF34 binding to b/PRT1 while preserving its contact with g/TIF35 *in vivo*. WCEs were prepared from H450 (*tif34Δ*) bearing wt *TIF34-HA* and empty vector (lanes 1 – 4), wt *TIF34-HA* and 8x His-tagged hc *TIF35* (lanes 5 – 8) and mutant *tif34-DD/KK-HA* and 8x His-tagged hc *TIF35* (lanes 9 – 12) and analyzed as in Figure 5A - B. (In) lanes contained 5% of the input WCEs; (E1) lanes contained 10% of eluate from the resin; (E2) lanes contained 20% of eluate from the resin; and (FT) lanes contained 5% of the flow through. (**B**) The *tif34-D207K* and *tif34-D224K* mutations are redundant and have only mild effect on the MFC composition *in vivo*. WCEs were prepared from YAH12 (*prt1Δ tif34Δ*) bearing untagged *PRT1* and wt *TIF34* on sc plasmids (lanes 1-3), or from YAH11 (*prt1Δ tif34Δ*) bearing 8x His-tagged *PRT1* and either wt *TIF34* (lanes 4-6), mutant *tif34-D207K* (lanes 7-9) or mutant *tif34-D224K* (lanes 10-12), and analyzed as in Figure 5A - B. (In) lanes contained 5% of the input WCEs; (E) lanes contained 100% of eluate from the resin; and (FT) lanes contained 5% of the flow through. (**C**) The *prt1-R678A* and *prt1-Y677A* mutations are redundant and have only mild effect on the MFC composition *in vivo*. WCEs were prepared from YAH06 (*prt1Δ*) bearing untagged *PRT1* (lanes 1 – 3), 8x His-tagged *PRT1* (lanes 4 – 6) and two of its mutant derivatives (lanes 7 – 9 and 10 - 12) and analyzed as in Figure 5A - B. (In) lanes contained 5% of the input WCEs; (E) lanes contained 100% of eluate from the resin; and (FT) lanes contained 5% of the flow through. (**D**) The *prt1-W674A* mutation provokes severe leaky scanning defect. The YAH06 (*prt1Δ*) strains bearing either wt

PRT1 or mutant *prt1-W674A* were transformed with the *GCN4-lacZ* reporter plasmids pM226 (i) and plig102-3 (ii), grown in SD medium at 34°C and analyzed as in Figure 6D.

Supplementary Table S1. Data collection and refinement statistics (MIR)

	D61 (native)	HgThioMer	Pt
Data collection[a]			
Space group	$P3_1$ 2 1	$P3_1$ 2 1	$P3_1$ 2 1
Cell dimensions			
a, *b*, *c* (Å)	126.28 126.28 105.64	125.9 125.9 105.45	125.9 125.9 107.58
α, β, γ (°)	90 90 120	90 90 120	90 90 120
Resolution (Å)	54.7-2.2 (2.32-2.2)[b]	75.8-2.99 (3.15-2.99)	54.5-3.8 (4-3.8)
R_{merge} (%)[c]	13.5	22.0	31.8
$\langle\langle I\rangle/\sigma(\langle I\rangle)\rangle$	10.2 (2.2)	9.3 (2.1)	2.9 (1.1)
Completeness (%)	99.9 (100)	97.5 (83.1)	99.9 (100)
Multiplicity	7.4 (7.6)	7.6 (7.3)	3.8 (3.7)
Wavelength (Å)	1.0000	1.5418	1.5418
Phasing			
Phasing power, acentric (Isomorphous/Anomalous)		0.98/0.21	0.25/0.05
Mean Figure of merit, acentric (inner resolution bin)	0.16 (0.81)		
<FoM> after solvent flattening (53%)	0.69		
Refinement			
No. reflections	47261		
R_{work} / R_{free} (%)	19/24		
No. atoms			
Protein	6145		
Water	237		
<B> factors (Å^2)			
Protein	37.6		
Water	38.9		
R.m.s. deviations			
Bond lengths (Å)	0.022		
Bond angles (°)	1.867		
Ramachandran plot (%)[d]			
Favoured	96.31		
Allowed	3.43		
Outliers	0.26		

[a] Data were collected on a single crystal, and in the refinement, 5% of unique reflections were removed as a test set for R_{free} calculation.

[b] Values in parentheses are for highest-resolution shell.

[c] $R_{merge} = \Sigma_{hl} | I_{hl} - \langle I_h \rangle | / \Sigma_{hl} \langle I_h \rangle$ where I_{hl} is the l^{th} measurement of reflection h.

[d] From MolProbity (29)

Supplementary Table S2. The i/TIF34-b/PRT1 interaction interface#

b/PRT1	Distance, Å	i/TIF34
Contacts involving side chains		
F:Tyr677 (OH)[a]	2.70	D:Asp224 (OD1)[a]
F:Arg678 (NH1)	3.49	D:Thr209 (OG1)
Main-chain contacts		
F:Phe694 (N)	3.35	D:Asp207 (OD2)
F:Met689 (O)	2.96	D:Lys164 (NZ)
Salt bridges		
F:Arg678 (NH1)	2.99	D:Asp207 (OD2)
F:Arg678 (NH2)	2.75	D:Asp207 (OD2)

[a] F, D is the chain id. Contacts in another complex from the ASU, between chains E and B are the same with minor distance deviations. The interaction parameters were calculated using PISA tool (35).

Table S3. Yeast strains used in this study

Strain	Genotype	Source or reference
YAH06	*MATa leu2-3,112 ura3-52 trp1Δ prt1::hisG GCN2* (hc *PRT1 URA3*)	(12)
AY134	*MATa leu2-3,112 ura3-52 trp1Δ prt1::hisG GCN2* (lc *PRT1 LEU2*)	This study
YAH11	*MATa leu2-3,112 ura3-52 trp1Δ prt1::hisG tif34Δ GCN2* (lc *PRT1-His LEU2* and hc *TIF34 URA3*)	This study
YAH12	*MATa leu2-3,112 ura3-52 trp1Δ prt1::hisG tif34Δ GCN2* (hc *PRT1,URA3* and sc *TIF34-HA TRP1*)	This study
H450	*MATa leu2-3,-112 ura3-52::GCN2 trp1Δ tif34Δ* (hc *TIF34 URA3*)	L. Cuchalová
H420	*MATa leu2-3, -112 ura3-52 trp1 gcn2Δ tif34Δ* (hc *TIF34 URA3*)	Klaus H. Nielsen
H417	*MATa leu2-3, -112 ura3-52 trp1*	Klaus H. Nielsen
H418	*MATa leu2-3, -112 ura3-52 trp1 gcn2Δ*	Klaus H. Nielsen

Table S4. Plasmids used in this study

Plasmid	Description	Source of reference
pRS-b/PRT1-HisXS	low copy wt *PRT1* in *LEU2* plasmid from pRS315	(12)
pRS-b/PRT1-W674A-His	low copy *PRT1* containing the *W674A* mutation in *LEU2* plasmid from pRS315	This study
pRS-b/PRT1-W674F-His	low copy *PRT1* containing the *W674F* mutation in *LEU2* plasmid from pRS315	This study
pRS-b/PRT1-Y677A-His	low copy *PRT1* containing the *Y677A* mutation in *LEU2* plasmid from pRS315	This study
pRS-b/PRT1-R678A-His	low copy *PRT1* containing the *R678A* mutation in *LEU2* plasmid from pRS315	This study
pRS-b/PRT1-Y677A-R678A-His	low copy *PRT1* containing *Y677A* and *R678A* mutations in *LEU2* plasmid from pRS315	This study
pRS-b/PRT1-Y677A-R678D-His	low copy *PRT1* containing *Y677A* and *R678D* mutations in *LEU2* plasmid from pRS315	This study
YEp-TIF34-U	high copy *TIF34 URA3* plasmid from YEplac195	(10)
YCp-i/TIF34-HA	single copy wt *TIF34-HA* in *LEU2* plasmid from YCplac111	(10)
YCp-i/TIF34-D207K-HA	single copy wt *TIF34-HA* containing the *D207K* mutation in *LEU2* plasmid from YCplac111	This study
YCp-i/TIF34-D224K-HA	single copy wt *TIF34-HA* containing the *D224K* mutation in *LEU2* plasmid from YCplac111	This study
YCp-i/TIF34-D207K-D224K-HA	single copy wt *TIF34-HA* containing *D207K* and *D224K* mutations in *LEU2* plasmid from YCplac111	This study
YCp-i/TIF34-L222D-HA	single copy wt *TIF34-HA* containing the *L222D* mutation in *LEU2* plasmid from YCplac111	This study
YCp-i/TIF34-L222K-HA	single copy wt *TIF34-HA* containing the *L222K* mutation in *LEU2* plasmid from YCplac111	This study
YCp-i/TIF34-HA-W	single copy wt *TIF34-HA* in *TRP1* plasmid from YCplac22	This study
YCp-i/TIF34-D207K-D224K-HA-W	single copy wt *TIF34-HA* containing *D207K* and *D224K* mutations in *TRP1* plasmid from YCplac22	This study
YCp-i/TIF34-D207K-HA-W	single copy wt *TIF34-HA* containing *D207K* mutation in *TRP1* plasmid from YCplac22	This study
YCp-i/TIF34-D224K-HA-W	single copy wt *TIF34-HA* containing *D224K* mutation in *TRP1* plasmid from YCplac22	This study
YEplac195	high copy *URA3* plasmid	(64)
YEp-g/TIF35	high copy wt *TIF35* in *URA3* plasmid from YEp352	(10)
YCp-g/TIF35-His-screen	single copy wt *TIF35-His* in *TRP1* plasmid from YCplac22	(5)
YEp-g/TIF35-His	high copy wt *TIF35-His* in *URA3* plasmid from YEplac195	This study
YEp-SUI1	high copy *SUI1* (eIF1) in *URA3* plasmid from YEplac195	(39)
pCFB130	high copy *sui1-His* containing the 93-97 mutation in *LEU2* plasmid form YEplac181	(47)
pJCB02	high copy *sui1-His* containing the D83G mutation in *LEU2* plasmid form YEplac181	(47)
pJCB04	high copy *sui1-His* containing the Q84P mutation in *LEU2* plasmid form YEplac181	(47)
pCFB134	high copy *sui1-His* containing the G107R mutation in *LEU2* plasmid form YEplac181	(47)
YEp-SUI1-G107R	high copy *sui1* containing the G107R mutation in *URA3* plasmid from YEplac195	This study
pGEX-5X-3	cloning vector for GST fusions	(63)

pGEX-i/TIF34	GST-i/TIF34 fusion plasmid from pGEX-5X-3	(10)
pGEX-g/TIF35	GST-g/TIF35 fusion plasmid from pGEX-5X-3	(10)
pGEX-b/PRT1	GST-b/PRT1 fusion plasmid from pGEX-5X-3	(13)
pGEX-RPS0A	GST-RPS0A fusion plasmid from pGEX-4T-1	This study
pT7-b/PRT1	*PRT1* ORF cloned under T7 promoter into pT7-7	(10)
pT7-b/PRT1-W674A	*PRT1* ORF containing the *W674A* mutation cloned under T7 promoter into pT7-7	This study
pT7-b/PRT1-Y677A	*PRT1* ORF containing the *Y677A* mutation cloned under T7 promoter into pT7-7	This study
pT7-b/PRT1-R678A	*PRT1* ORF containing the *R678A* mutation cloned under T7 promoter into pT7-7	This study
pT7-i/TIF34	*TIF34* ORF cloned under T7 promoter into pT7-7	(10)
pT7-i/TIF34-D207K-D224K	*TIF34* ORF containing *D207K* and *D224K* mutations cloned under T7 promoter into pT7-7	This study
pM226	Derivative of pM199; ORF of uORF1 extends into the *GCN4-lacZ* coding region	(61)
plig102-3	Low copy *URA3* vector with *GCN4* leader point mutations containing uORF4 only at its original position in front of the *GCN4-lacZ* coding region	(61)

Table S5. Primers used in this study

Primer name	Primer sequence (5´to 3´)
AH-PRT1-BamHI	TCACTTGGGATCCATCTGGTA
AH-PRT1-NotI-R	CGCGGTGGCGGCCGCGGATCT
AH-PRT1-W674A-R	TGCTTGCTTCAATAATTCACGTTG
AH-PRT1-W674A	CAACGTGAATTATTGAAGCAAGCAACCGAATATAGAGAAAAAATT
AH-PRT1-W674F-R	GAATTGCTTCAATAATTCACGTTG
AH-PRT1-W674F	CAACGTGAATTATTGAAGCAATTCACCGAATATAGAGAAAAAATT
AH-PRT1-YR-AA-R	TTTTTCCATTTCTTGGCCAATTTTTTCTGCTGCTTCGGTCCATTGCTTCAATAA
AH-PRT1-YR-AD-R	TTTTTCCATTTCTTGGCCAATTTTTTCATCTGCTTCGGTCCATTGCTTCAATAA
AH-PRT1-Y677A-R	TTCCATTTCTTGGCCAATTTTTTCTCTTGCTTCGGTCCATTGCTTCAA
AH-PRT1-R678A-R	TTCCATTTCTTGGCCAATTTTTTCTGCATATTCGGTCCATTGCTTCAA
y3iKpnI	TACTTTGGATGGTCACACCGGTACCAT
BmgBIr	CGGCCTTCTCCACGTCGTATTTGAAAT
D207K	GTGACATGCAATTTTCTCCTAAGTTAACATACTTTATTACATCATCCAGAGATA
D207Kr	AGGAGAAAATTGCATGTCACTGATGGA
D224K	ATACTAACTCGTTCTTGGTCAAGGTATCGACTCTACAAGTTCTTAAGAAATACG
D224Kr	GACCAAGAACGAGTTAGTATCTCTGGA
LC3iL222D	ACATCATCCAGAGATACTAACTCGTTCGACGTCGATGTATCGACTCTACAAGTTCTT
LC3iLr	GAACGAGTTAGTATCTCTGGATGATGT
LC3iL222K	ACATCATCCAGAGATACTAACTCGTTCAAGGTCGATGTATCGACTCTACAAGTTCTT
O1-BamHI	AATAGGATCCCATATGTCCTTACCAGCTACTTTTGAC
BSRPS0Aexon1-r	TGAAAACATACGGTTCTTGGTGAACTTGAACGTTTCTAGCAC
BSRPS0Aexon2	CAAGAACCGTATGTTTTCAACGCAAGACC
O2-KpnI-XhoI-r	TTCTCGAGATGGTACCACTTACCACTCGACGTTGTCAGCATTTTC

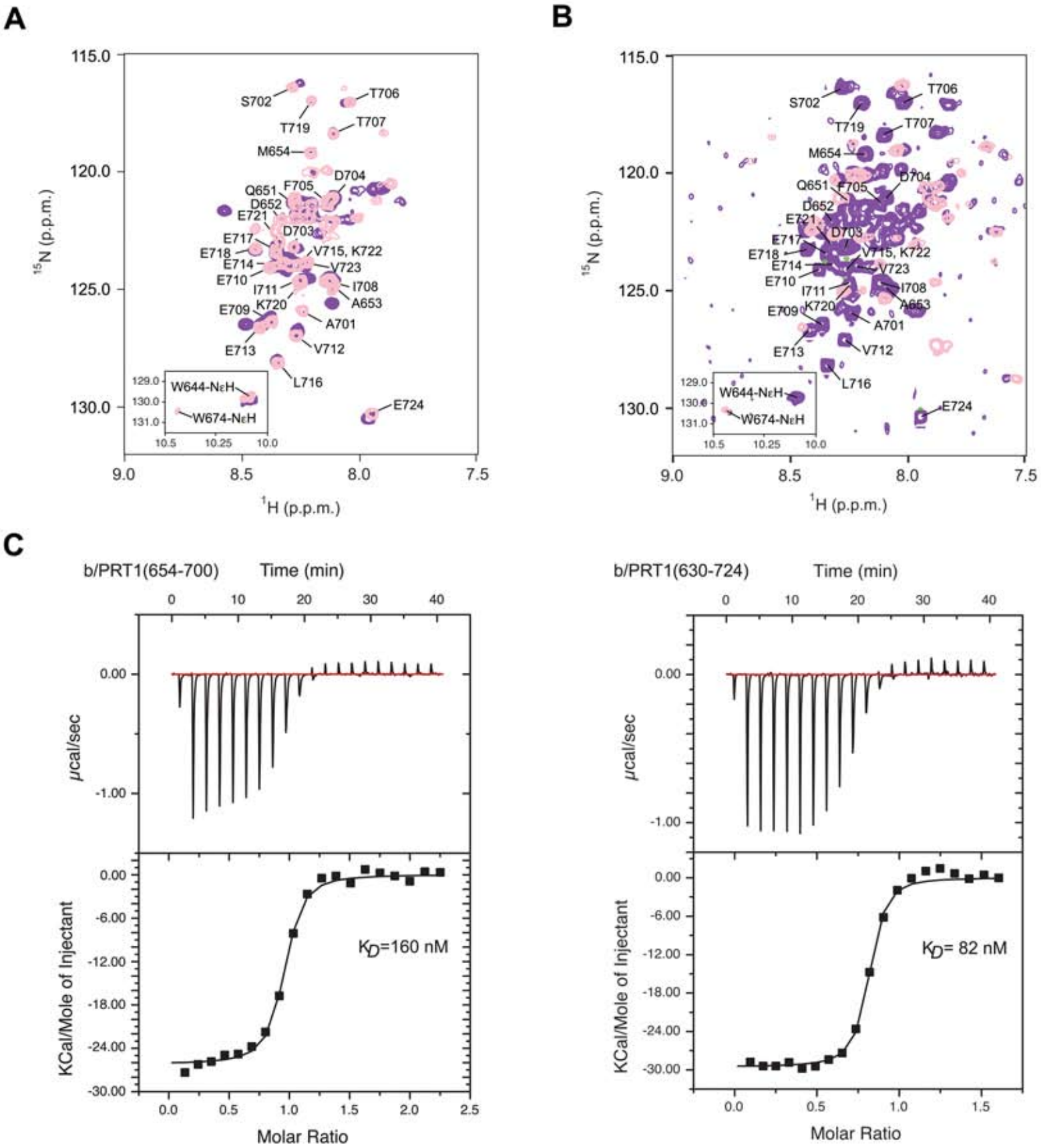
A
B
C
^{15}N (p.p.m.)
^{1}H (p.p.m.)
S702
T706
T719
T707
M654
D704
Q651
F705
D652
E721
D703
E717
E718
V715, K722
E714
V723
E710
I711
I708
A653
E709
K720
A701
E713
V712
L716
E724
W644-NεH
W674-NεH
b/PRT1(654-700)
Time (min)
μcal/sec
KCal/Mole of Injectant
Molar Ratio
K_D=160 nM
b/PRT1(630-724)
K_D= 82 nM

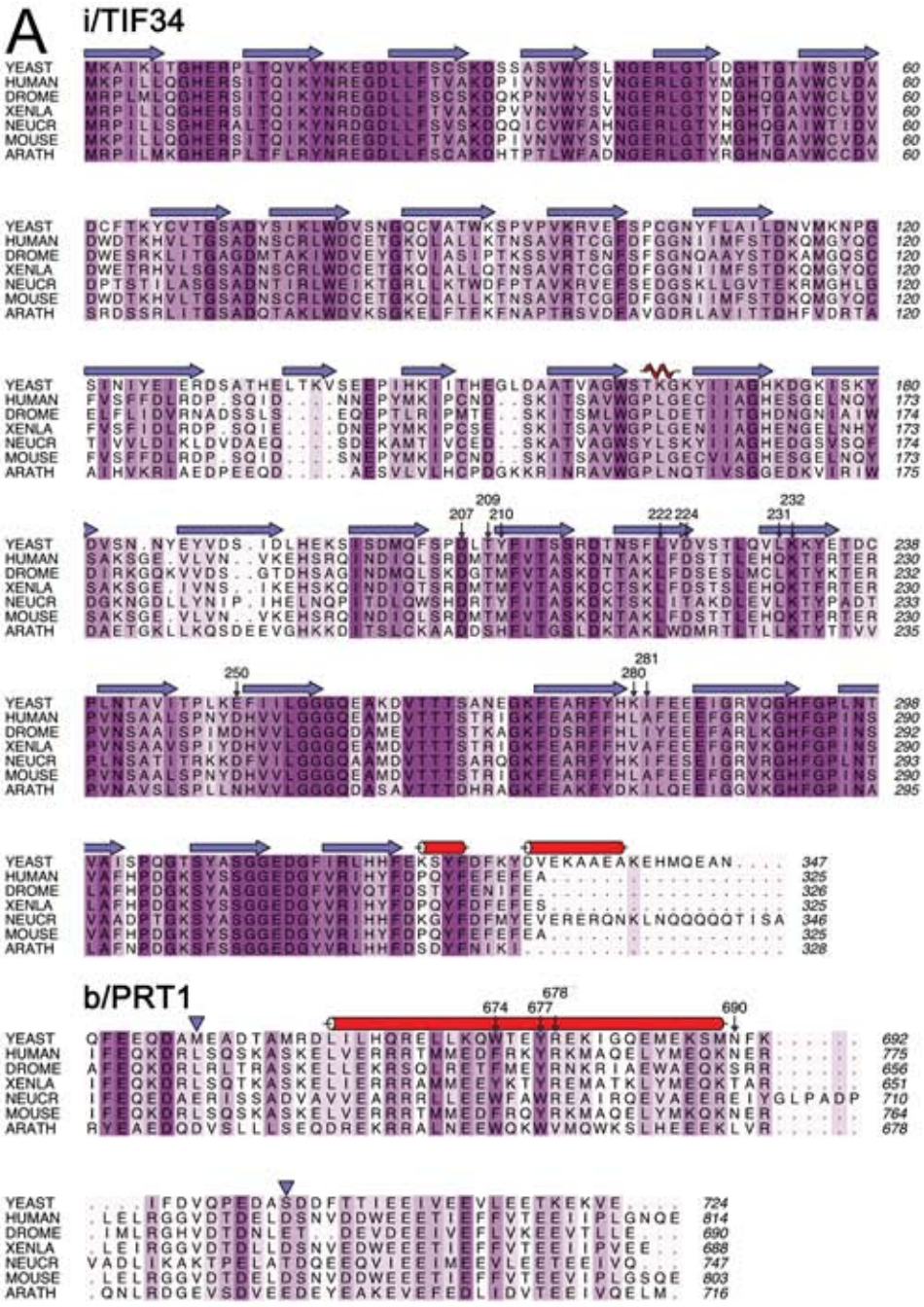
A
i/TIF34
YEAST
HUMAN
DROME
XENLA
NEUCR
MOUSE
ARATH
b/PRT1
YEAST
HUMAN
DROME
XENLA
NEUCR
MOUSE
ARATH

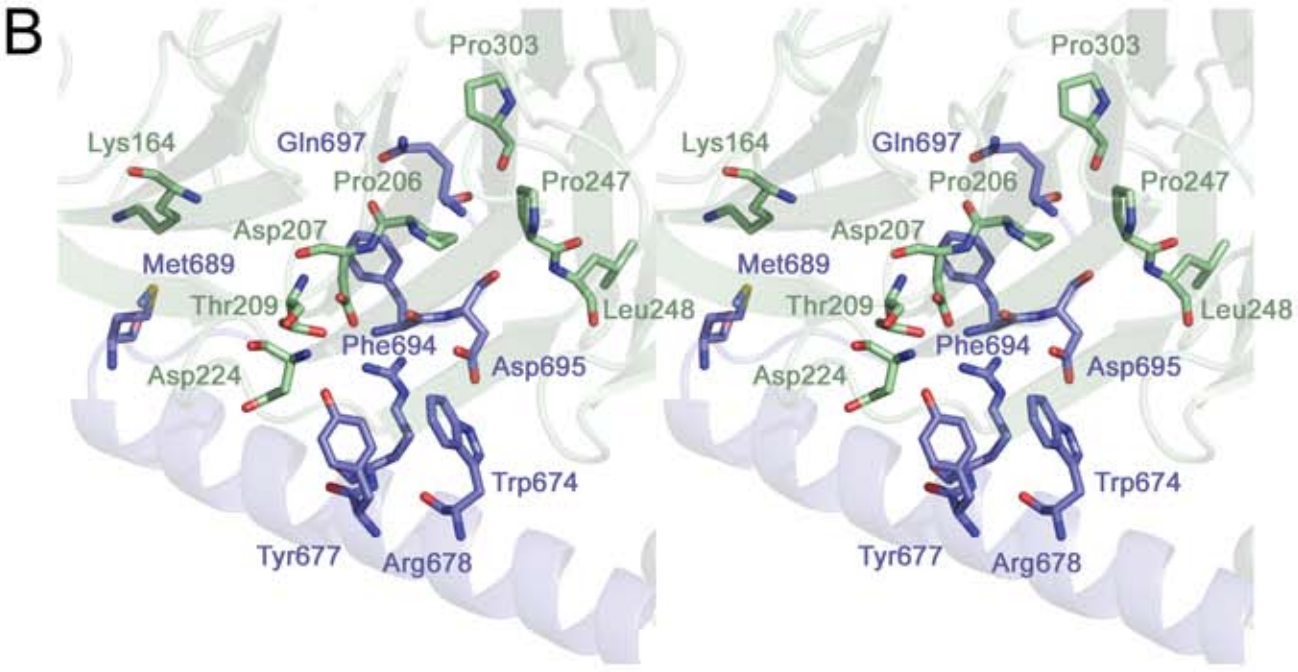
B
Pro303
Lys164
Gln697
Pro206
Pro247
Asp207
Met689
Thr209
Leu248
Phe694
Asp695
Asp224
Trp674
Tyr677
Arg678

A

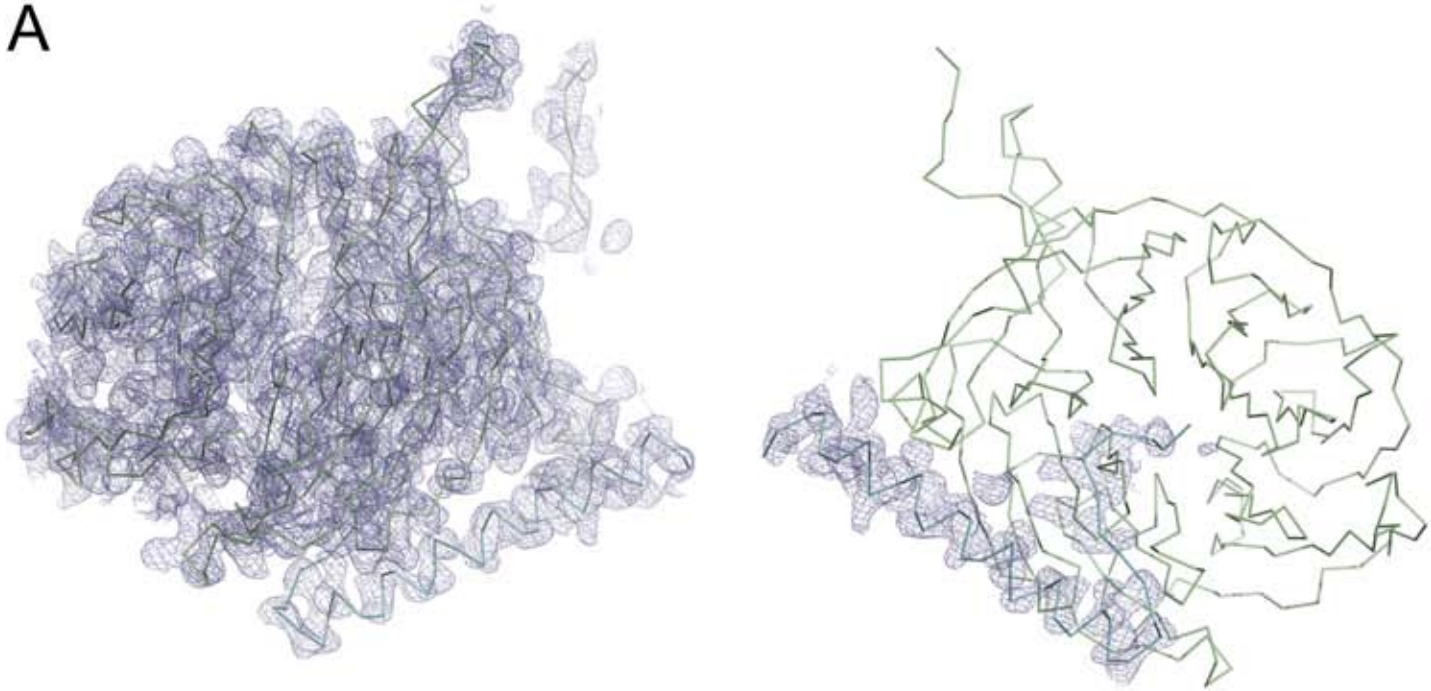

B

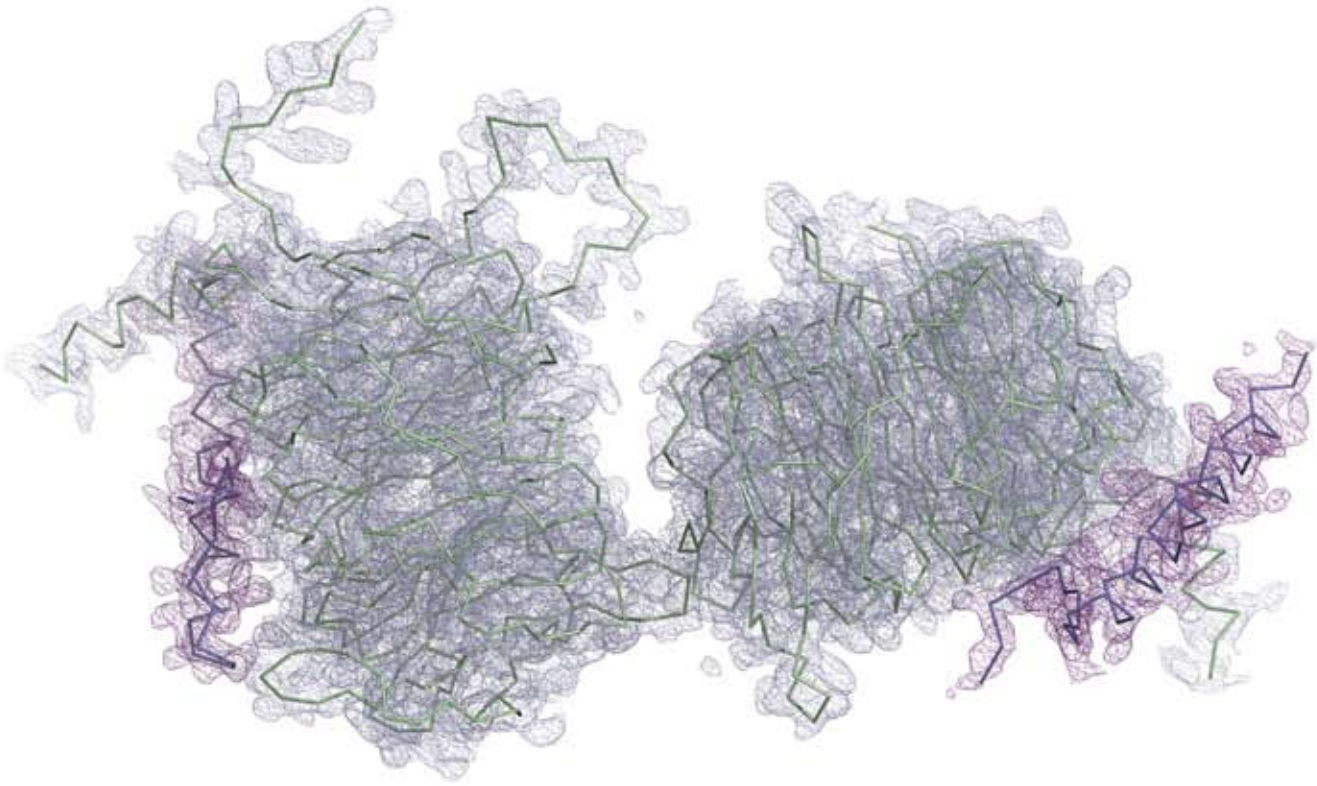

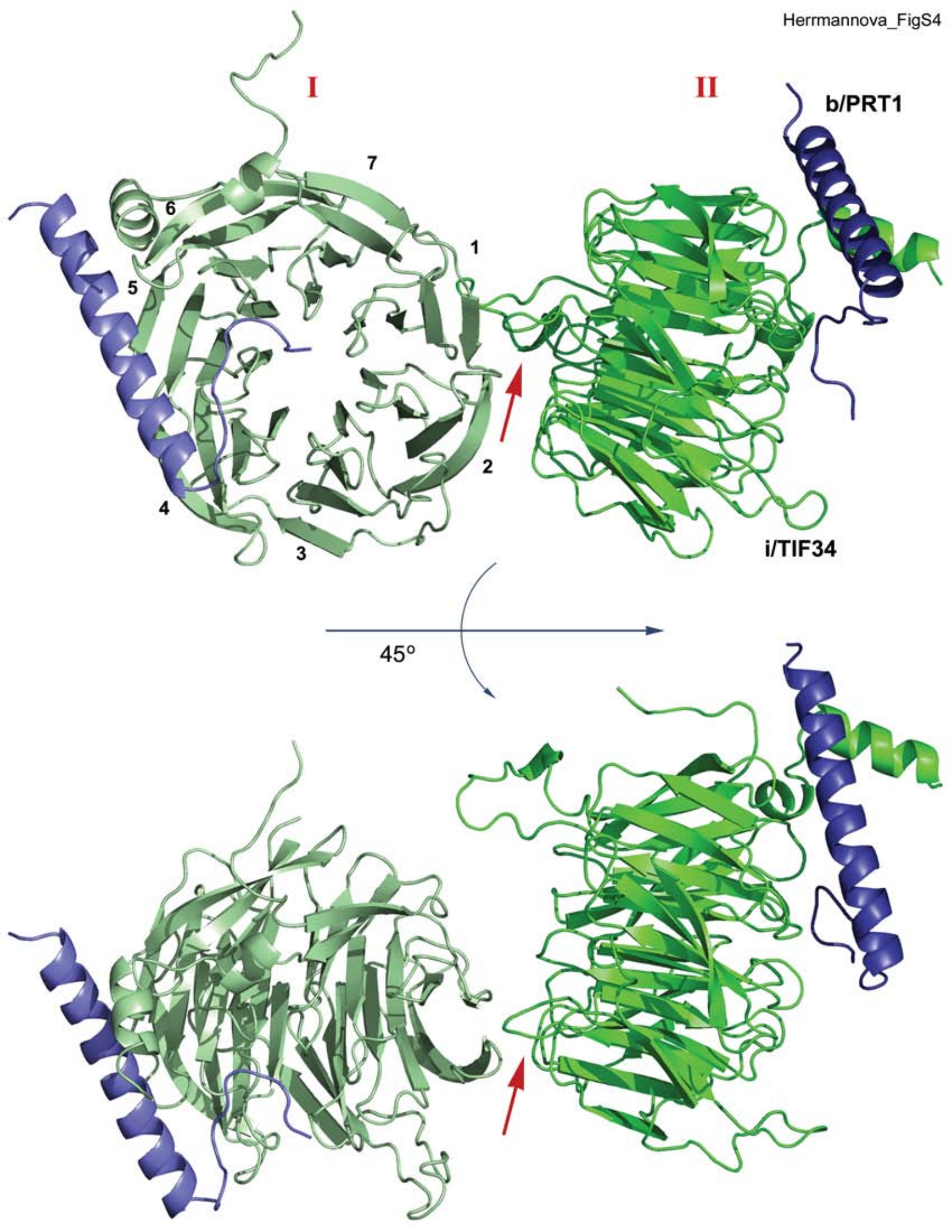
I
II
b/PRT1
7
6
1
5
2
4
3
i/TIF34
45°

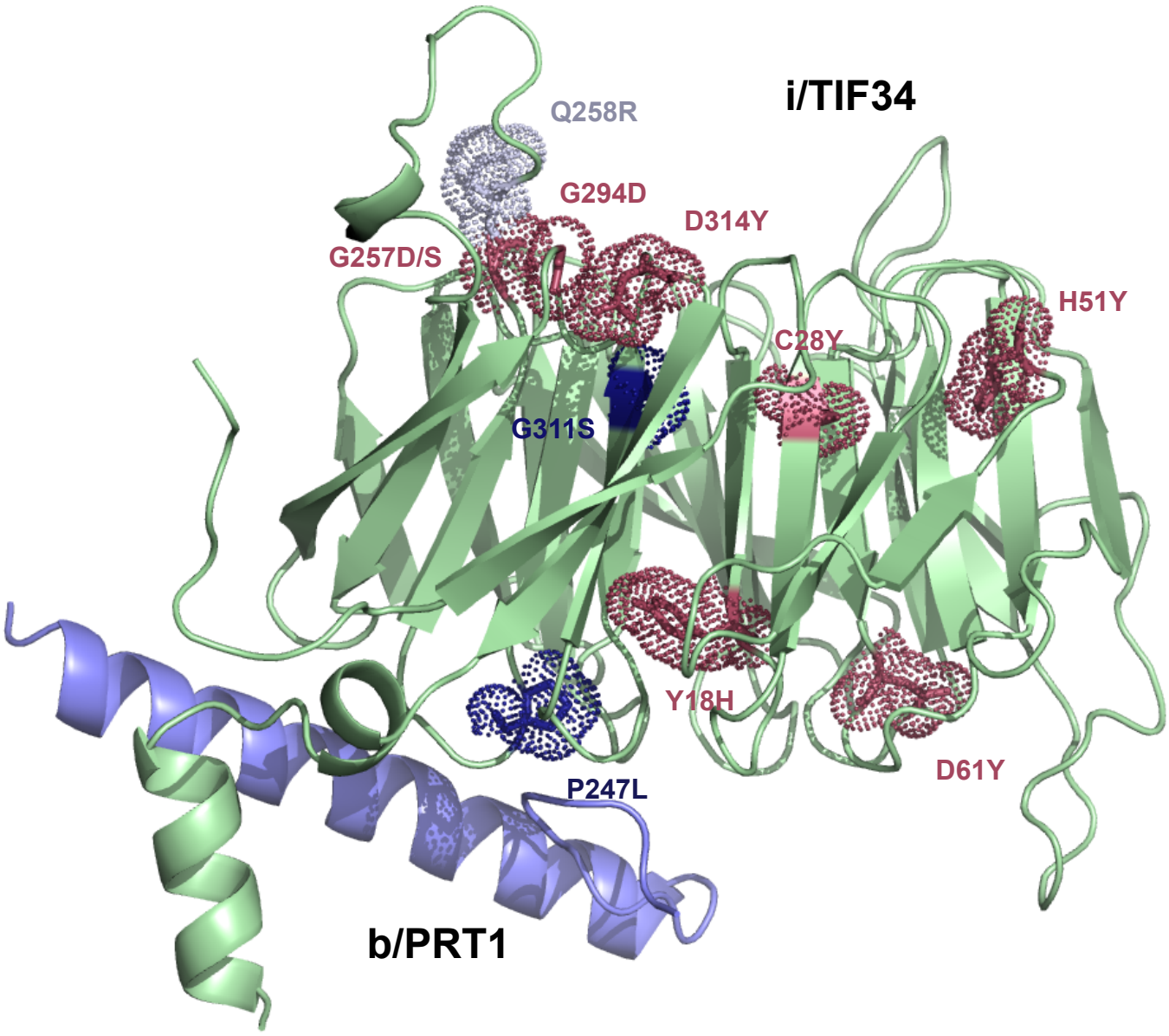
i/TIF34
Q258R
G294D
D314Y
G257D/S
H51Y
C28Y
G311S
Y18H
D61Y
P247L
b/PRT1

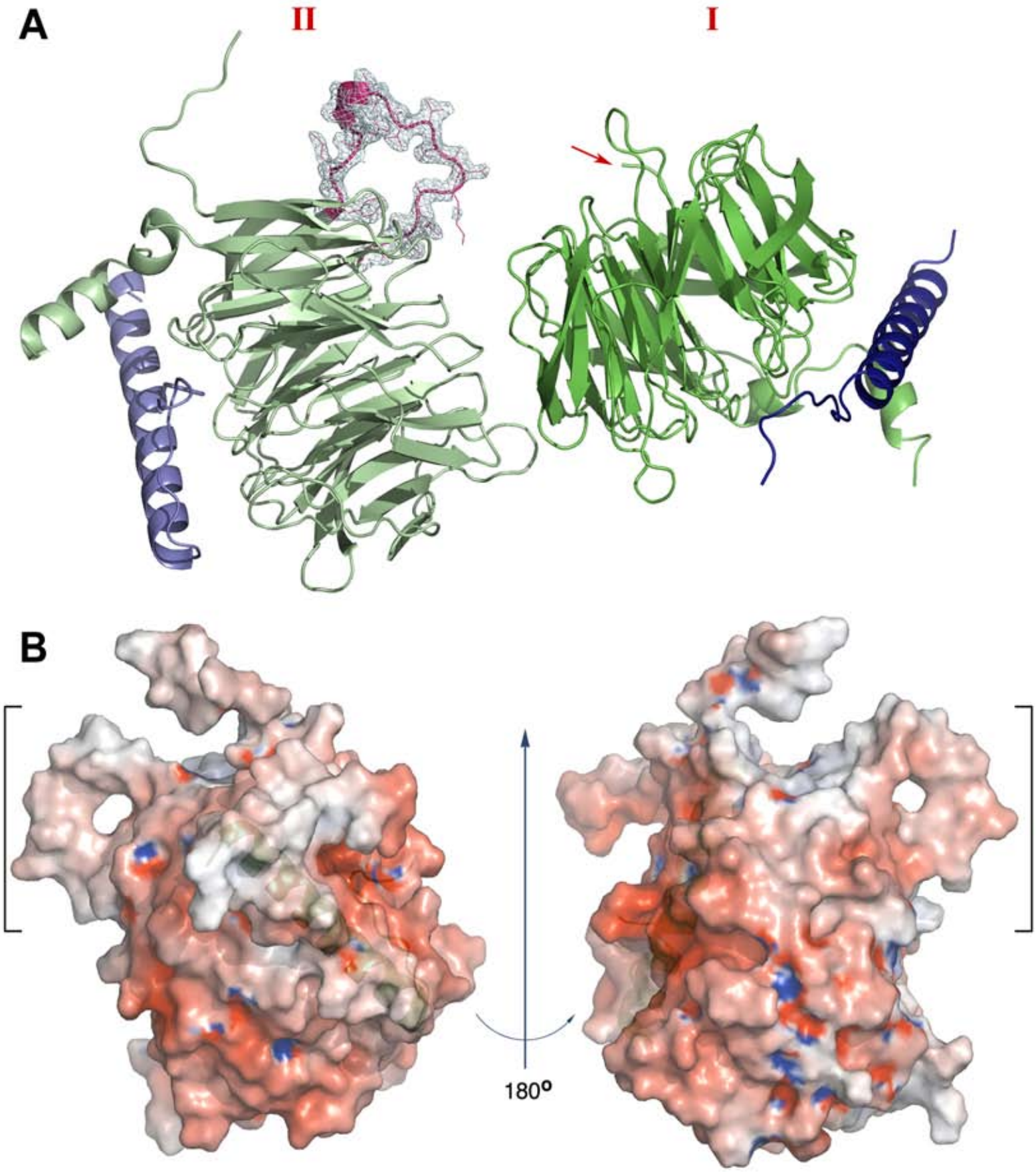
A
II
I
B
180°

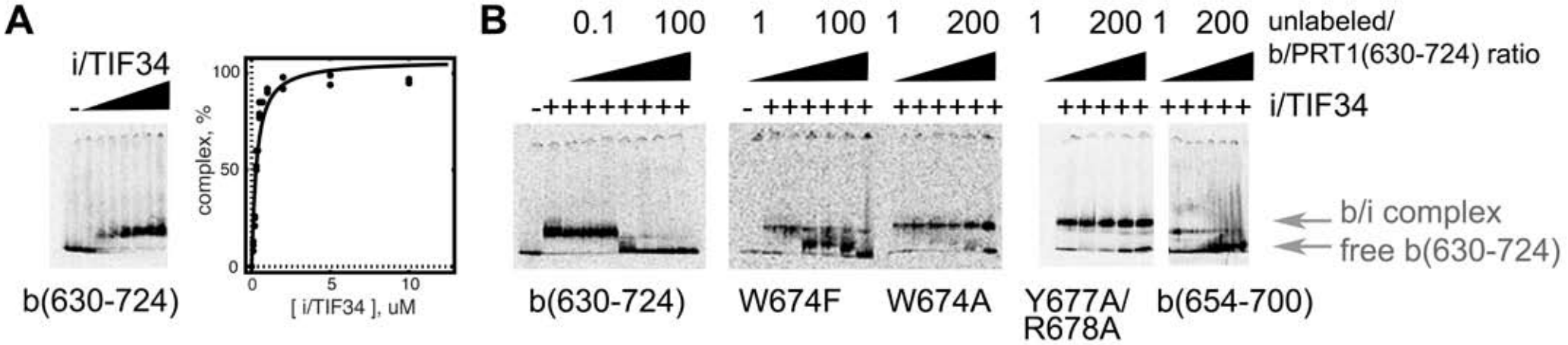
A
i/TIF34
-
b(630-724)
complex, %
100
50
0
0
5
10
[i/TIF34], uM
B
0.1
100
1
100
1
200
1
200
1
200
unlabeled/
b/PRT1(630-724) ratio
-++++++++
- ++++++
++++++
+++++
+++++
i/TIF34
b/i complex
free b(630-724)
b(630-724)
W674F
W674A
Y677A/
R678A
b(654-700)

A

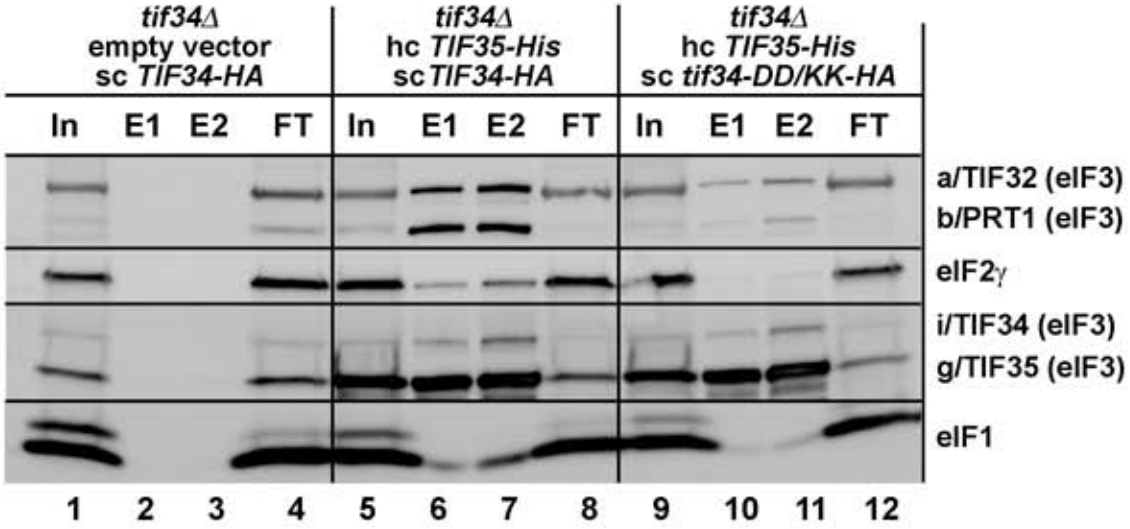

B

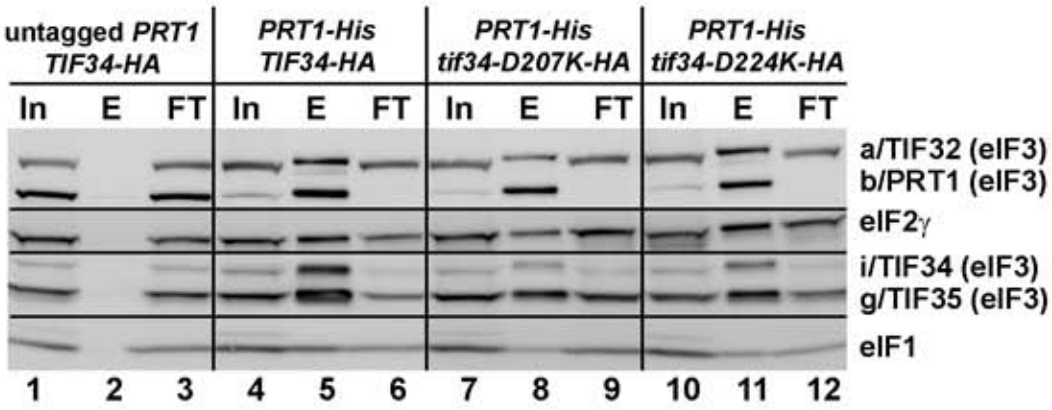

C

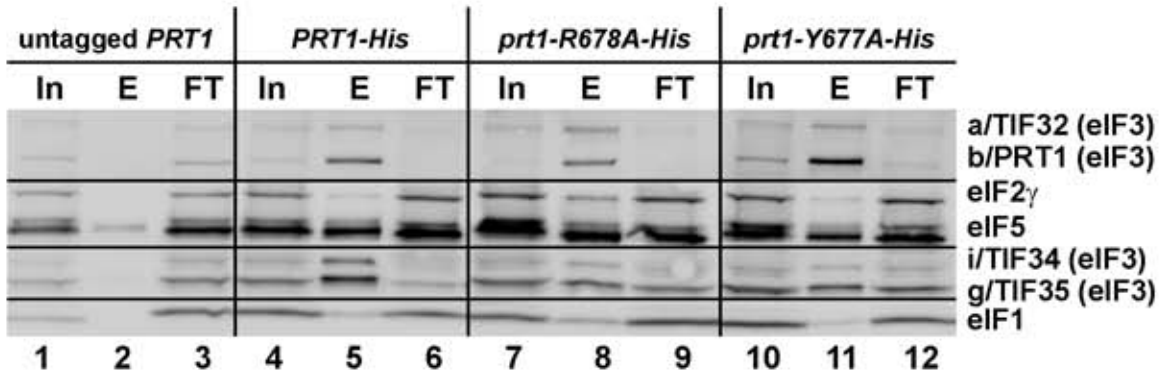

D

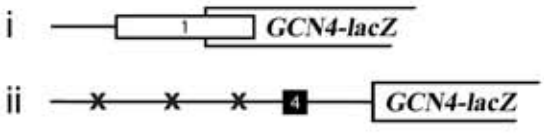

PRT1	*prt1-W674A*
10±1 **1x**	139±6 **13.9x**
42±3 **1x**	278±17 **6.6x**

Units of β-Galactosidase Activity
Activity relative to WT